Blending of phased array data

Duijster, Arno; Van Groenestijn, Gert Jan; Van Neer, Paul; Blacquière, Gerrit; Volker, Arno

DOI
10.1063/1.5031562

Publication date
2018

Document Version
Final published version

Published in
44th Annual Review of Progress in Quantitative Nondestructive Evaluation, Volume 37

Blending of phased array data

Cite as: AIP Conference Proceedings **1949**, 080005 (2018); https://doi.org/10.1063/1.5031562
Published Online: 20 April 2018

Arno Duijster, Gert-Jan van Groenestijn, Paul van Neer, Gerrit Blacquière, and Arno Volker

Blending of Phased Array Data

Arno Duijster[1, a)], Gert-Jan van Groenestijn[1], Paul van Neer[1], Gerrit Blacquière[1,2], and Arno Volker[1]

[1] *TNO, Oude Waalsdorperweg 63, P.O. box 96864, 2509 JG The Hague, The Netherlands.*
[2] *Delft University of Technology, Geotechnology Department, Section of Applied Geophysics and Petrophysics, Delft, The Netherlands.*

[a)] Corresponding author: arno.duijster@tno.nl

Abstract. The use of phased arrays is growing in the non-destructive testing industry and the trend is towards large 2D arrays, but due to limitations, it is currently not possible to record the signals from all elements, resulting in aliased data. In the past, we have presented a data interpolation scheme 'beyond spatial aliasing' to overcome this aliasing. In this paper, we present a different approach: blending and deblending of data. On the hardware side, groups of receivers are blended (grouped) in only a few transmit/recording channels. This allows for transmission and recording with all elements, in a shorter acquisition time and with less channels. On the data processing side, this blended data is deblended (separated) by transforming it to a different domain and applying an iterative filtering and thresholding. Two different filtering methods are compared: f-k filtering and wavefield extrapolation filtering. The deblending and filtering methods are demonstrated on simulated experimental data. The wavefield extrapolation filtering proves to outperform f-k filtering. The wavefield extrapolation method can deal with groups of up to 24 receivers, in a phased array of 48 × 48 elements.

INTRODUCTION

Phased arrays are commonly used in various fields of engineering and science. In ultrasound nondestructive testing applications, they can be used to inspect large sections of an object in a relatively short time. Nowadays, the number of elements in those phased arrays is increasing. The need for larger two-dimensional arrays is motivated by the desire to cover larger areas while maintaining the same spatial resolution, in order to decrease costs; or to improve the spatial resolution by decreasing the element spacing, in order to increase quality.

However, this growth of array size comes at a cost. Regarding hardware, all array elements have to be wired properly, leading to large wire bundles; all recorded data has to be acquired simultaneously leading to large data acquisition systems; and all data has to be stored and processed properly. Beside these hardware drawbacks, limitations can also appear in data acquisition procedures, for instance when it is not feasible to emit signals from all sources independently, or to record signals from all receivers sequentially, due to time constraints, leading to aliased data.

A solution to these problems can be the use of only a (random) subset of the elements from the whole array, record only those signals, and apply a data interpolation scheme in order to estimate the missing data from the elements left out from the subset. We have presented this method at the QNDE 2015 and 2016 conferences [1,2]. A different approach is to use all elements, but connect random subsets of receivers (referred to as 'blending') in order to reduce the number of measurement signals. Recording those blended signals ensures that all data is still present but mixed up, requiring a deblending procedure in order to obtain estimates of all individual receivers.

DATA MODELING

Our interest in blending of phased array data originates from the field of seismic surveying [3,4], and the method can easily be applied to ultrasonic nondestructive testing. Before dealing with the blending and deblending procedures

44th Annual Review of Progress in Quantitative Nondestructive Evaluation, Volume 37
AIP Conf. Proc. 1949, 080005-1–080005-10; https://doi.org/10.1063/1.5031562
Published by AIP Publishing. 978-0-7354-1644-4/$30.00

themselves, the data modeling needs to be defined. The basic setup consists of a set of sources and a set of receivers at known positions on the surface of the medium to be inspected. After emission of signal by one or more sources, the wave propagates through the medium, is scattered within the medium, propagates back to the surface, and can be recorded by the receivers. This is shown schematically in Fig. 1 for a single source and single receiver. For each frequency, the resulting response **P** of the acoustic transmission from all sources to all receivers can be written as

$$\mathbf{P} = \mathbf{D}\ \mathbf{X}\ \mathbf{S}\,, \tag{1}$$

where the **S** and **D** matrices represent the frequency response of the source and of the receiver, respectively [5]. The matrix **P** has the dimensions $n_{rec} \times n_{src}$, i.e. the number of receivers n_{rec} times the number of sources n_{src}. This matrix operation, as well as all others in this paper, are performed for each frequency independently. For notational simplicity, the source position (x_s, y_s, z_0), receiver position (x_r, y_r, z_0), and frequency ω are left out. The response of the medium **X** is subsequently written as

$$\mathbf{X} = \textstyle\sum_i [\mathbf{W}^-(z_0, z_i)\ \mathbf{R}(z_i, z_i)\ \mathbf{W}^+(z_i, z_0)]\,, \tag{2}$$

where $\mathbf{W}^+(z_i, z_0)$ and $\mathbf{W}^-(z_0, z_i)$ are the forward and backward wave propagation through the medium, and $\mathbf{R}(z_i, z_i)$ is the response of the medium at depth z_i, summed over all depths or diffractors. For notational simplicity, source and receiver positions and frequency have been left out again.

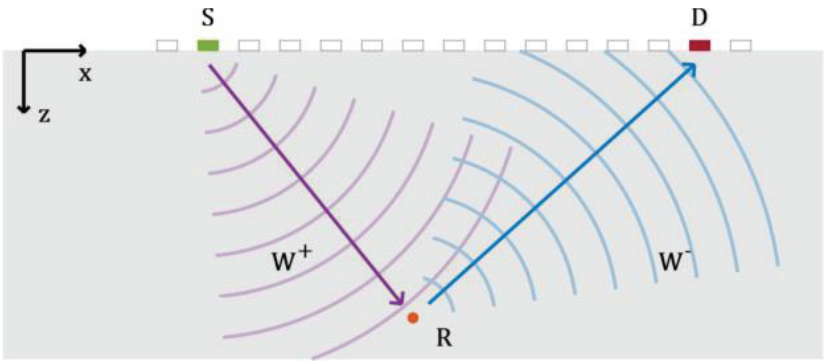

FIGURE 1. A schematic overview of the wave propagation modelling, showing the path from a source **S** via a diffractor **R** to a receiver **D**. The third spatial dimension (y) points inward.

BLENDING

The main focus in this paper is on blending and deblending of receiver signals. Although the theory applies equally well to blending of sources, or even to blending of both sources and receivers, this will not be dealt with here. Note that due to hardwiring of receivers, the configuration becomes fixed and cannot be changed for sources and receivers independently, or in between experiments.

The blending factor b is the number of elements combined into a single data acquisition channel, or in other words the number of receivers n_{rec} divided by the number of available channels n_{ch}. After choosing a specific factor, the receivers are randomly divided over the required channels, with the restriction that all receivers blended to a single channel must be located at least a defined separation distance from each other. The blending factor is chosen to be constant for the whole array, leading to subsets which are equally large.

The measured output signal from the array of receivers is a multi-dimensional data structure, depending on the spatial position of the source and of the receivers, as well as of time. A blending operator **Γ** is constructed, which is a very sparse array of dimensions $n_{ch} \times n_{rec}$, leading to the summation of the receiver signals into the proper channel, as

$$\mathbf{P}_{bl} = \mathbf{\Gamma}\ \mathbf{P}\,, \tag{3}$$

where **P** and $\mathbf{P}_{bl}$ are respectively the response of all (unblended) signals (of size $n_{rec} \times n_{src}$), and the blended response (of size $n_{ch} \times n_{src}$). Figure 2 shows an example of a blending with factor 12, decreasing the number of 576 elements to 48 acquisition channels.

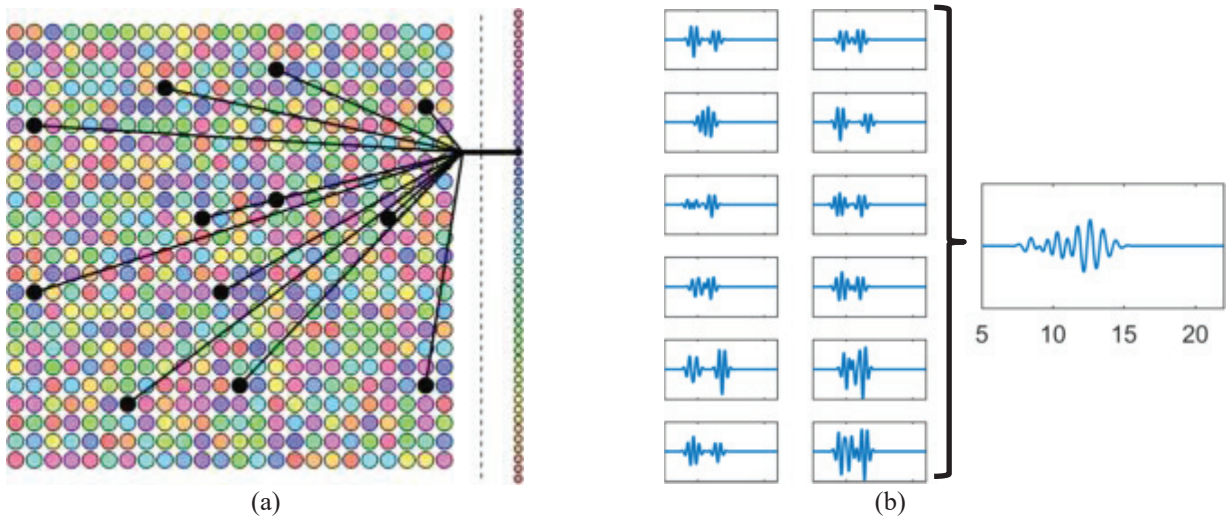

(a) (b)

FIGURE 2. An example of blending: (a) all receivers are divided into random subsets, and each subset is connected into one data acquisition channel, illustrated in black for a single subset; (b) the 12 individual receiver signals of that particular subset are not recorded separately, but only the superpositioned signal, on the right.

DEBLENDING

After recording all channels, the data has to be deblended in order to obtain estimations of the signals of the individual receiver elements. Since the blending operator $\mathbf{\Gamma}$ contains more columns than rows ($n_{rec} > n_{ch}$), inversion is not possible, due to non-existence of $\mathbf{\Gamma}^{-1}$. A first estimation can be obtained by pseudo-deblending. Since this is not the optimal solution, an iterative procedure is engaged in order to improve the estimation.

Pseudo-deblending aims to restore the original size of the data matrix from the reduced-size blended data matrix, as

$$\mathbf{P}_{ps} = \mathbf{\Gamma}^{\mathrm{H}} \, \mathbf{P}_{bl} \, . \tag{4}$$

In this pseudo-deblending step, the blended signal from each single acquisition channel is mapped onto all corresponding receivers. This means that the rightmost, blended signal in Fig. 2b is assigned to all twelve (black) receivers in Fig. 2a. As a result, the pseudo-deblended data matrix $\mathbf{P}_{ps}$ has the correct size, and it contains the true data, but it is corrupted with pseudo-deblending noise. For a single element, the pseudo-deblending noise consists of the contributions of the $b - 1$ other signals blended into the same channel, as can be seen in Fig. 3.

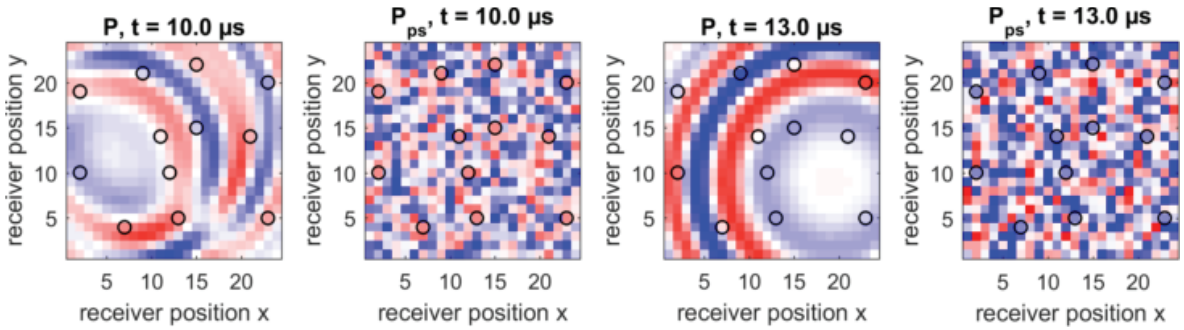

(a) (b) (c) (d)

FIGURE 3. An example of pseudo-deblending of the blended data from Fig. 2: (a) and (c) are true signals at two different time steps, and (b) and (d) are the corresponding pseudo-deblended results, showing the pseudo-deblending noise. Note that the amplitudes of all 12 connected elements (circles) are identical in the pseudo-deblended images.

Iterative Scheme

In order to decrease the pseudo-deblending noise, an iterative loop is used. Within this loop an estimation of the noise is obtained and subtracted from the pseudo-deblended data. A schematic overview of this iterative procedure is shown in Fig. 4.

The procedure is as follows:

1. Record blended data $\mathbf{P}_{bl}$. The true data $\mathbf{P}$ is unknown, and the blending operator has to be known.
2. Perform a pseudo-deblending to obtain $\mathbf{P}_{ps}$.
3. Start at iteration $i = 0$; define $\widehat{\mathbf{N}}^{(0)} = 0$.
4. Subtract the estimated interference $\widehat{\mathbf{N}}^{(i)}$ from $\mathbf{P}_{ps}$ in order to obtain an improved estimation $\widehat{\mathbf{P}}^{(i)}$.
5. Evaluate whether the stop criterion is met; if not, continue with step 6, else finish with step 10.
6. Filter this estimation in order to (further) reduce the noise, and obtain $\widehat{\mathbf{P}}_f^{(i)}$.
7. Perform a blending and a pseudo-deblending on the filtered estimation and obtain $\widehat{\mathbf{P}}_{f,ps}^{(i)}$.
8. Obtain an estimation of the pseudo-deblended noise, or interference, defined as $\widehat{\mathbf{N}}^{(i)} = \widehat{\mathbf{P}}_{f,ps}^{(i)} - \widehat{\mathbf{P}}_f^{(i)}$.
9. Increase the iteration counter by one and continue with step 4.
10. End with an estimation $\widehat{\mathbf{P}}$ of the true data $\mathbf{P}$.

Most steps in this loop are straight forward mathematics (subtraction or matrix multiplication), only the filtering step can be optimized. The quality of the filtering determines the quality of the final results. Two filtering approaches are considered for the moment: f-k filtering, and wavefield extrapolation.

In the filtering part of the iterative loop, a threshold parameter α is included, which is decreased as function of the iteration number. This decreasing threshold leads to a gradual filtering out of the pseudo-deblending noise.

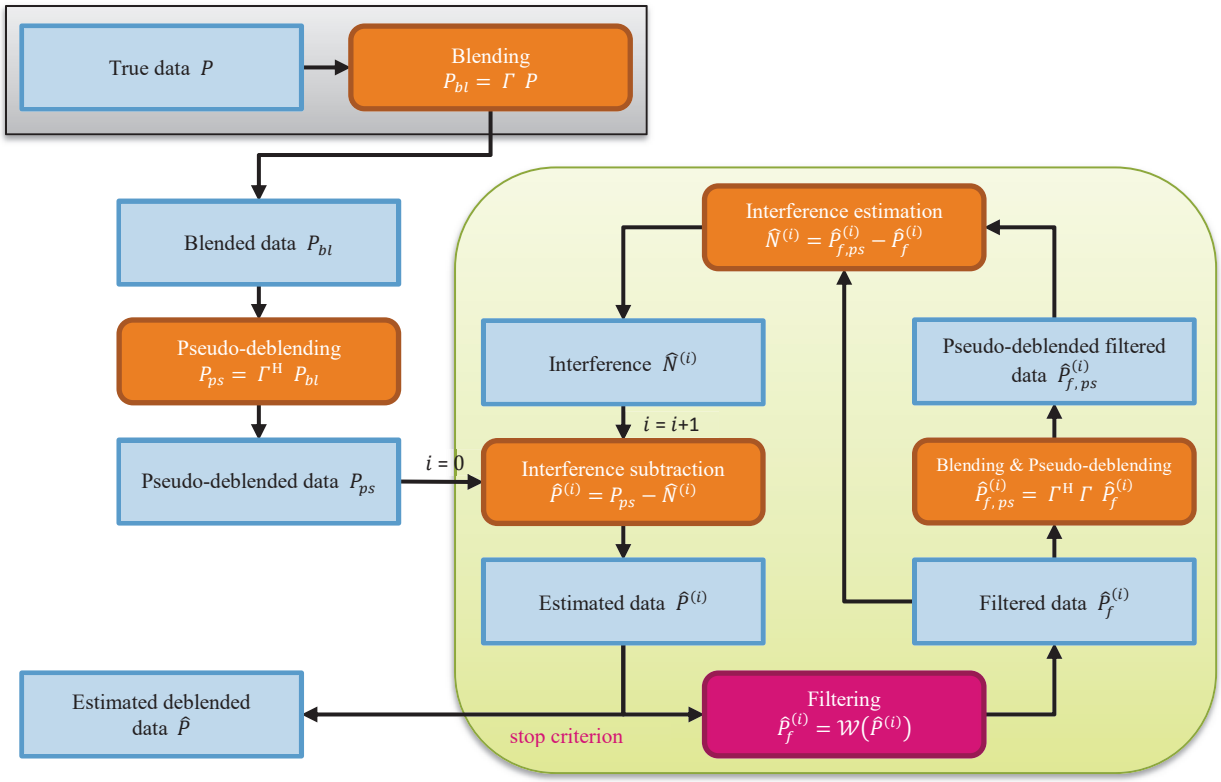

FIGURE 4. A schematic overview of the iterative deblending procedure.

f-k Filtering

The noise which appears due to pseudo-deblending is assumed to be incoherent, in contrast with the true signals which are coherent. As a result, the noise is spread out over all wavenumber and frequency components in the frequency domain. The noise can be reduced by masking the data, zeroing all contributions with a wave velocity above a certain threshold value or with frequencies outside an interval. A truncated cone-shaped mask $\mathbf{M}$ in the three-dimensional space $(f,\ k_x, k_y)$ can be defined as

$$\mathbf{M} = \begin{cases} 1 & \text{if } \left(f > c_{\text{lim}}\sqrt{k_x^2 + k_y^2}\right) \wedge (f_{min} \leq f \leq f_{max}) \\ 0 & \text{otherwise} \end{cases}, \tag{5}$$

where f, k_{x}, and k_{y} are respectively the temporal frequency and the two wavenumber dimensions, c_{lim} is the velocity threshold (i.e. minimum velocity in the medium) and f_{min} and f_{max} are frequency limitations. This process is illustrated in Fig. 5. After transformation back to the spatial/temporal domain, the result is thresholded with the aforementioned threshold α.

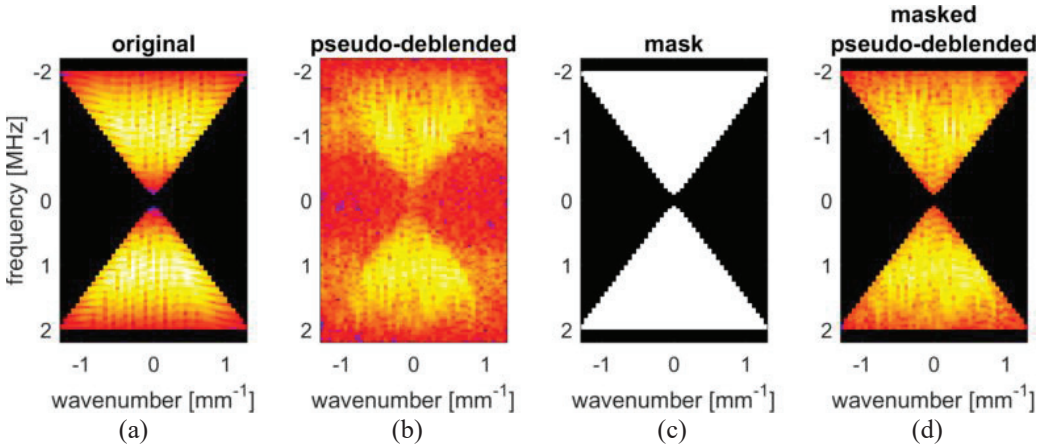

FIGURE 5. A cross-section in the frequency domain (frequency versus one of the two wavenumber dimensions), showing (a) the true data, (b) the blended and pseudo-deblended data, (c) the mask, and (d) the mask applied to the pseudo-deblended data.

Wavefield Extrapolation Filtering

A second approach in filtering is based on wavefield extrapolation. Again, it is assumed that the noise due to pseudo-deblending is incoherent. Since the true data is assumed to originate from diffractors in the medium, the expected signals are shaped as hyperboloids. This means that by inverse wavefield extrapolation, the signals can be focused, by

$$\mathbf{P}_{foc} = (\mathbf{W}^{-})^{\text{H}}\ \mathbf{P}\ . \tag{6}$$

Since the true signals are now more focused than before the operation, their energy is more condensed, and the non-focused noise can be filtered out by thresholding. After thresholding with the aforementioned threshold α, the process can be reversed by a forward wavefield extrapolation ($\mathbf{P} = \mathbf{W}^{-}\ \mathbf{P}_{foc}$) can be applied to restore the correct arrival times. This process is illustrated in Fig. 6.

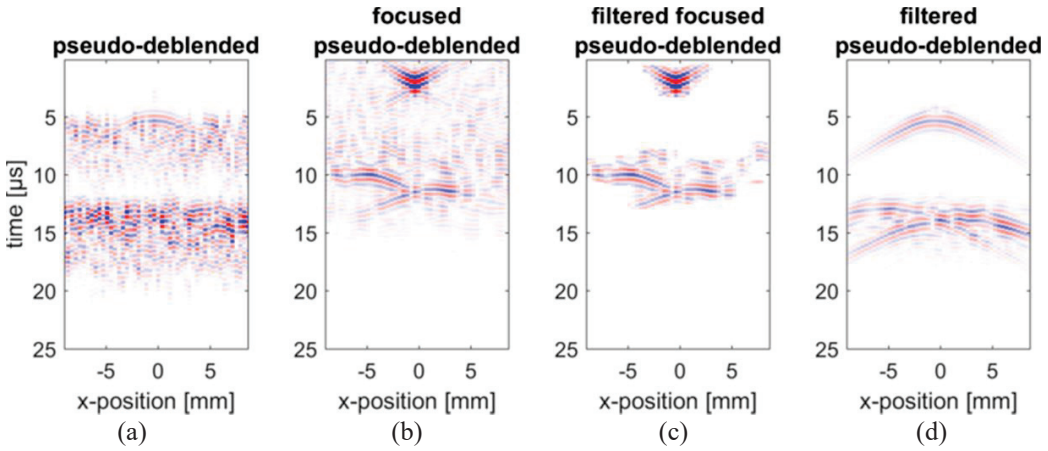

FIGURE 6. A cross-section in the temporal domain at $y = 0$ mm, showing (a) the pseudo-deblended data, (b) the focused pseudo-deblended data, (c) a thresholded version of (b), and (d) the inverse focussing applied.

NUMERICAL EXAMPLE

The validation and comparison of the method has been performed on a simulated experiment. An equidistant, square grid of 48 × 48 receivers has been defined, with a spacing of 0.375 mm, shown in Fig. 7. The medium is water, and three diffractors are placed at different depths and with different scattering strengths. The source is placed in the center of the surface, emitting a 1 MHz pulse. An example of the measured (unblended!) data cube is shown in Fig. 8, where the response of each receiver position (x_r, y_r) is shown as function of time t.

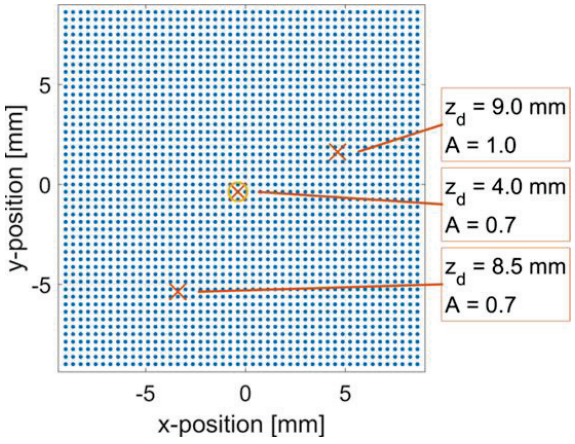

FIGURE 7. A top-view of the simulation setup. The dots represent the 2304 receivers, the crosses the horizontal positions of the diffractors, with in text their depths and scattering strengths; and the circle represents the source.

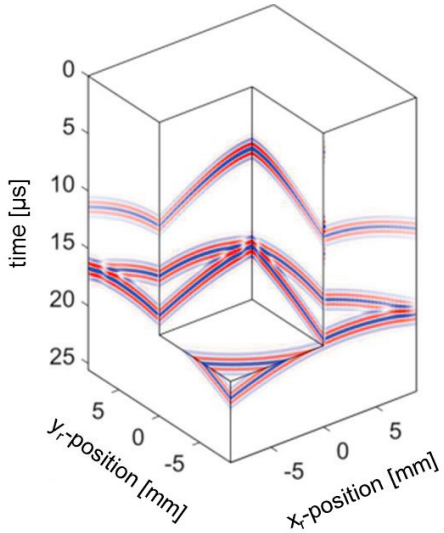

FIGURE 8. A graphical representation of the data cube $\mathbf{p}(x_r, y_r, t)$, as function of the receiver positions (x_r, y_r) and time t. The hyperboloidal shapes of each of the three diffractors can be distinghuished.

Blending factor

A first experiment is the variation of the blending factor. The main question is to what factor the deblending will lead to a reasonably good restoration of the unblended signal. Comparison is done qualitatively. Results of a blending and deblending with factors $b = 4$, $b = 8$ and $b = 12$ are shown in Fig. 9. In the pseudo-deblended signal the three hyperbolas are not distinguishable, and but with both filtering methods these are restored. Note that the results are obviously better for lower blending factors, since less noise has to be removed. The results of the f-k filtering are decreasing in quality at a factor of 8, and at a factor of 12 it begins failing to restore the true signal. The wavefield extrapolation method still shows good quality results for all three cases, and a smoother image compared with the f-k filtering.

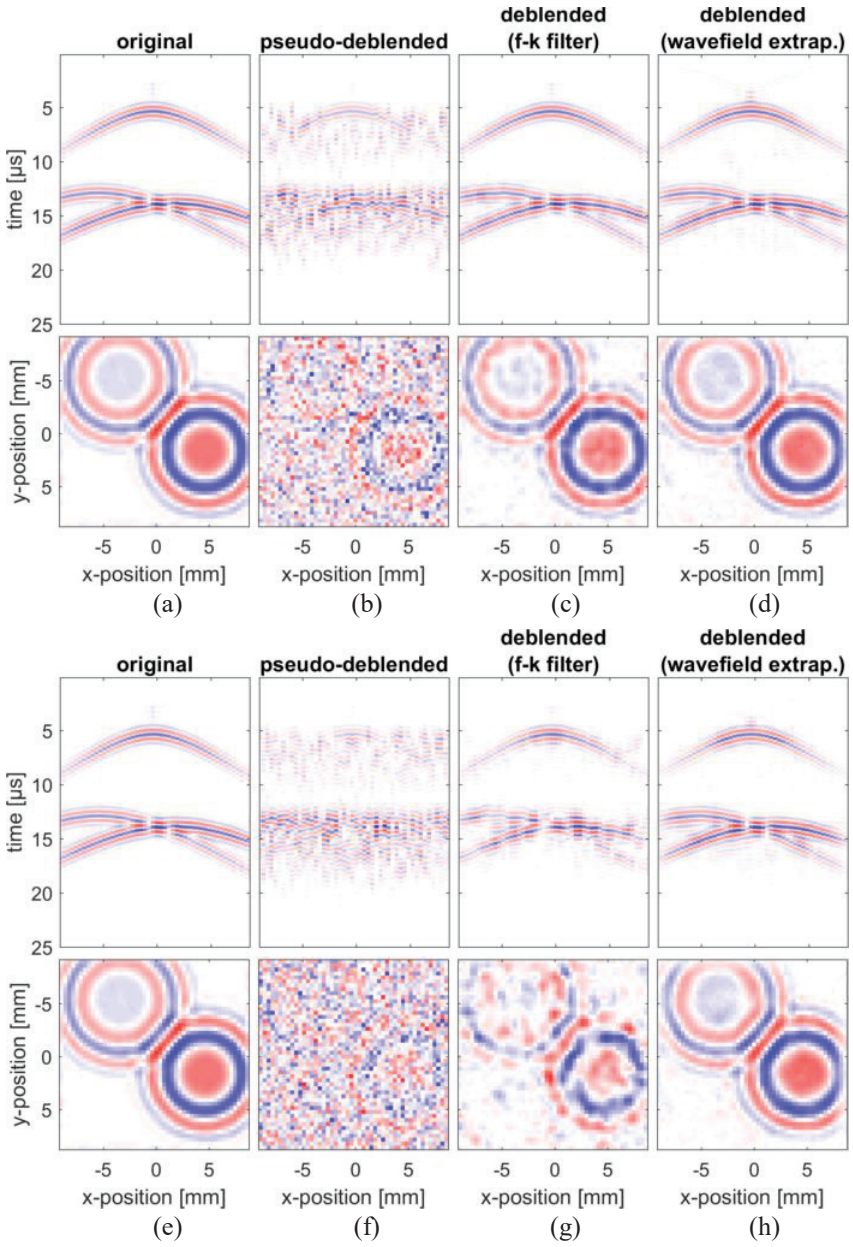

Blending factor 4

Cross-section at $y = 0$ mm

Cross-section at $t = 12$ µs

Blending factor 8

Cross-section at $y = 0$ mm

Cross-section at $t = 12$ µs

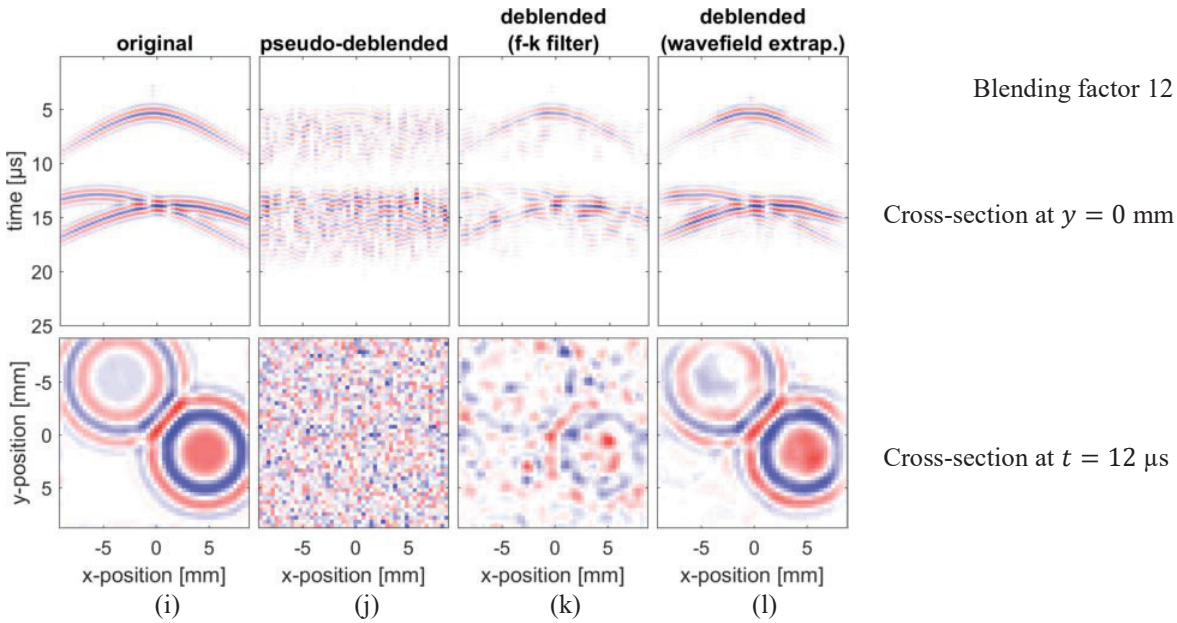

FIGURE 9. The results of the experiment with a blending factor of 4 (a)-(d), 8 (e)-(h) and 12 (i)-(l). The first column (a), (e) and (i) shows the unblended original signal, the second column (b), (f) and (g) the pseudo-deblended result with the noise obscuring the true signal, the third column (c), (g) and (k) the results of the iterative procedure using f-k filtering and the fourth column (d), (h) and (l) the results of the wavefield extrapolation filtering. Each subplot shows a cross-section at $y = 0$ mm (top rows) and a cross-section at $t = 12$ μs (bottom rows).

Sensitivity

The previous experiments have been performed using a fixed setup with three diffractors at a fixed position. In order to test the sensitivity to a specific setup, a series of experiments has been performed in which the number of diffractors, their positions and scattering strengths has been varied. Since the f-k filtering is performing less than the wavefield extrapolation filtering, only the latter method is used in this sensitivity test.

The number of diffractors in the medium has been increased from 1 up to 10, and 30 independent realizations of their position, depth and scattering strengths (all from uniform distributions) have been used as inputs for the data simulation. The simulated data are used in a blending/deblending experiment in which four blending factors have been taken into account: 4, 6, 8 and 12. In order to be able to compare these results quantitatively, an error metric has been defined as

$$\varepsilon = \frac{\|\boldsymbol{p_0} - \widehat{\boldsymbol{p}}\|}{\|\boldsymbol{p_0}\|} \tag{7}$$

where $\boldsymbol{p_0}$ is the unblended signal and $\widehat{\boldsymbol{p}}$ is the estimation after iterative filtering.

Results are shown in Fig. 10. The mean curves are almost flat, meaning that the error is only minorly dependent on the number of diffractors in the medium. The standard deviation is low but significant, indicating that position and scattering strength are of influence on the final result. Furthermore, it can be seen that the mean error increases with the blending factor, which is expected since the amount of pseudo-deblending noise increases with the blending factor.

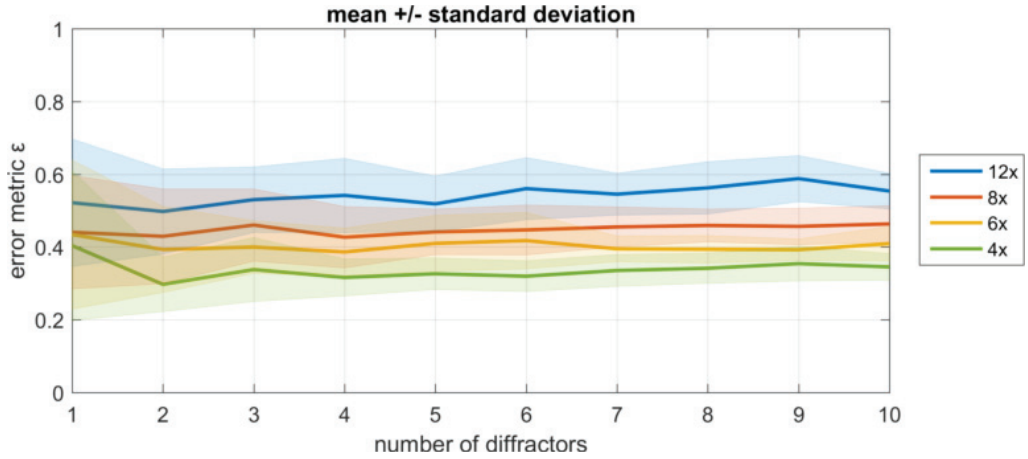

FIGURE 10. Results of the sensitivity test for the wavefield extrapolation method. The line shows the mean of the 30 experiments, and the shaded area shows the mean plus or minus one standard deviation.

Pushing the Limit

In the previous sections, the blending factor has been less than or equal to 12. But what is the result of even higher blending factors? How far can the blending go? For the same initial setup, the blending factor has been increased from 12 up to 48 (only divisors of the array length are allowed in the current implementation), and results are shown in Fig. 11. As can be seen, at a factor of 16, the individual hyperbolas still can be distinguished, but the results are becoming less smooth. At 24×, the hyperbolas are hardly visible and at 48× they have been filtered out with the noise. Which factor is still good, depends on the application. If only the number and position of diffractors have to be estimated, then 24× can still be a good start, but if smooth images are required, then 12× is possibly the limit.

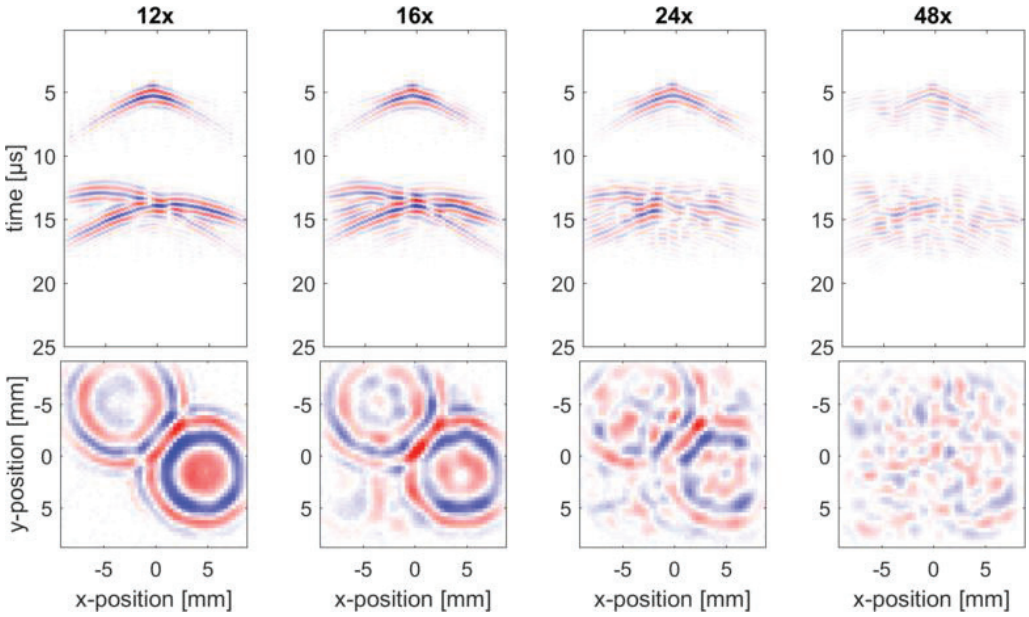

FIGURE 11. Results of wavefield extrapolation filtering on datasets with a high blending factors: 12, 16, 24 and 48, respectively.

CONCLUSIONS

Blending and deblending of data is a promising approach to overcome hardware limitations and time constraints, and still obtain alias-free data. A method has been presented to perform the deblending in an iterative scheme, alternating data filtering and noise estimation, after an initial pseudo-deblending step. Two filtering methods have been compared, both assuming the incoherency of the pseudo-deblending noise. It has been demonstrated that wavefield extrapolation filtering outperforms f-k filtering. The wavefield extrapolation method can deal with blending factors up to 24, in a phased array of 48 × 48 sources/receivers.

The presented blending and deblending method leaves room for improvement. The crucial filtering step in the iterative loop can be improved for instance by using imaging methods. The blending has to be studied into more detail. So far, a fixed factor has been used with random subsets. A varying factor (i.e. multiple subsets with varying blending factors), and optimization of the division into subsets can be topics of further study. Finally, simulation experiments with more complex media and realistic sources, and experimental validation is required in order to show the full potential of this technique.

REFERENCES

1. A. Volker, and P. van Neer, "Imaging beyond aliasing", in 42nd Annual Review of Progress in Quantitative Nondestructive Evaluation, eds. D. E. Chimenti, and L. J. Bond, AIP Conference Proceedings 1706, 020009 (2016).
2. A. Volker, and P. van Neer, "Data Interpolation beyond aliasing", in 43rd Annual Review of Progress in Quantitative Nondestructive Evaluation, eds. D. E. Chimenti, and L. J. Bond, AIP Conference Proceedings 1806, 020020 (2017).
3. A. Mahdad, P. Doulgeris, and G. Blacquière, "Separation of blended data by iterative estimation and subtraction of blending interference noise", Geophysics, 76(3): Q9–Q17 (2011).
4. C. Reinicke Urruticoechea, G.J.A. van Groenestijn, and G. Blacquière, "Seismic Blending and Deblending in 3D", 78th EAGE Conference and Exhibition (2016)
5. A. Berkhout, Seismic Migration: Imaging of Acoustic Energy by Wave Field Extrapolation, Part A: Theoretical Aspects, Elsevier (1982).